We are IntechOpen,
the world's leading publisher of
Open Access books
Built by scientists, for scientists

6,900
Open access books available

185,000
International authors and editors

200M
Downloads

154
Countries delivered to

Our authors are among the

TOP 1%
most cited scientists

12.2%
Contributors from top 500 universities

BOOK CITATION INDEX
CLARIVATE ANALYTICS
INDEXED

WEB OF SCIENCE™

Selection of our books indexed in the Book Citation Index
in Web of Science™ Core Collection (BKCI)

Interested in publishing with us?
Contact book.department@intechopen.com

Numbers displayed above are based on latest data collected.
For more information visit www.intechopen.com

High Precision and Fast Functional Mapping of Brain Circuitry through Laser Scanning Photostimulation and Fast Dye Imaging

Xiangmin Xu
The Department of Anatomy and Neurobiology, the University of California, Irvine
The United States of America

1. Introduction

The development of modern neuroscience tools has a significant impact on the progress in the field of neuroscience (Kandel, 1982). New tools has greatly faciliated the neuroscience resreach, and can be critical for studies of brain circuit organization and function. Although many approaches are useful by themselves, it is desirable to combine existing powerful techniques to harness each technique's advantages and compensate for limitations.

In many brain areas, neuronal circuits are segregated into anatomically discrete areas such as specific lamina and modules or compartments (Mountcastle, 1997). Functional imaging of these brain areas is particularly useful in characterizing circuit properties. Fast voltage-sensitive dye (VSD) imaging, which detects neuronal membrane potential changes via shifts in the dye absorption /or fluorescence emission in response to varying membrane potentials, offers a great means of simultaneous monitoring neuronal activities from many locations with high spatial and temporal resolutions. With new dyes and modern imaging apparatus, VSD imaging has been widely used to study spatiotemporal dynamics of population neuronal activity in cortical tissue both in vivo and in vitro (Grinvald & Hildesheim, 2004). Particularly, for in vitro brain slices, fast VSD imaging is important for mapping circuit organization and response dynamics, and more recently has been used to probe functional abnormalities in models of neurological and psychiatric disorders (Ang et al., 2006; Airan et al., 2007). One major limitation of most in vitro VSD imaging studies, however, lies in that the imaged neuronal responses are either spontaneous seizure activities through pharmacological manipulations or induced by electric stimulations (Petersen & Sakmann, 2001; Huang *et al.*, 2004; Ang *et al.*, 2006). Significant disadvantages of electric stimulation include indiscriminate activation of axons of passage, slow and inefficient placement of multiple stimulation locations, and tissue damage. In comparison, optical stimulation including laser scanning photostimulation (LSPS) either by glutamate uncaging or direct activation of light-sensitive channels (e.g., channelrhodopsin-2) enables rapid and noninvasive photoactivation of neurons with great convenience and superior spatial resolution in practical experiments (Callaway & Katz, 1993; Boyden *et al.*, 2005; Petreanu *et al.*, 2009). Combining whole-cell recordings from single neurons with photostimulation of clusters of presynaptic neurons permits extensive mapping of local functional inputs to individually recorded neurons (Schubert *et al.*, 2003; Shepherd & Svoboda, 2005; Xu & Callaway, 2009).

While both methods of VSD imaging and LSPS are already well established, the combination can offer new and potentially valuable advantages in studies of spatiotemporal dynamics and functional connectivity of populations of neurons in cortical circuits. LSPS does not activate the axons of passage and avoids the difficulty of restricted and unambiguous stimulation by electrode-based methods; VSD imaging affords the ability of reporting the information of population responses that is largely missed when the combination of photostimulation with single cell recordings is used for circuit input mapping. Although it is of great advantage to combine both VSD imaing and LSPS for circuit studies, the combination had never achieved due to technical challenges until recently my research group succeeded in this implemention. We have developed a new mapping technique that uses LSPS to provide precise and strong stimulation of neural circuit components, and allows for functional connectivity and spatiotemporal dynamics of population activity in large cortical areas to be examined by fast VSD imaging (Xu et al., 2010). This novel approach is an all-optical approach for brain circuit mapping, and it enables fast mapping and high-precision evaluation of cortical organization and function.
In this book chapter, I will report on this novel technique in detail, and introduce the system design and new technical improvement. Then I will describe effective applications of the technique in mapping brain circuitry.

2. General system design, calibration, VSD response characterization

2.1 The system design for combining LSPS with VSD imaging
Our overall system is illustrated in Figure 1, consisting of LSPS, VSD imaging, and electrophysiological recording systems. We adopted the design of the LSPS system described previously (Shepherd *et al.*, 2003; Shepherd & Svoboda, 2005). A laser unit (model 3501; DPSS Lasers, Santa Clara, CA) was used to generate 355 nm UV laser for glutamate uncaging. The laser beam was 1.5 mm in diameter and directed through the optical path of our system. Short durations of laser flashes (e.g., 1- 3 ms) were controlled by using an electro-optical modulator (i.e., pockels cell) (Conoptics, Danbury, CT) and a mechanical shutter (Uniblitz; Vincent Associates, Rochester, NY). Laser beam power was modulated by a neutral density gradient wheel and monitored by diverting a small fraction of the laser beam with a glass coverslip to a photodiode. The laser scanning system included an X-Y pair of scan mirrors, the scan lens, the tube lens, and the objective lens (Figure 1). The mirrors delivered the laser beam through a scan lens; then the beam entered the microscope (BX51WI; Olympus) via a dichroic mirror (351DRLP; Chroma Technology, Brattleboro, VT) and was focused by a custom-made UV-transmitting tube lens. The beam underfilled the back aperture of the microscope objective to provide a more columnar (as opposed to conical) illuminating beam, keeping the mapping as two-dimensional as possible by reducing the axial resolution. Various laser stimulation positions could be achieved through galvanometers-driven XY scanning mirrors (Cambridge Technology, Cambridge, MA), as the mirrors and the back aperture of the objective were in conjugate planes, translating mirror positions into different scanning locations at the objective lens focal plane. During uncaging, a variable number of patterned sites that covered the mapping field were stimulated sequentially in a nonraster, nonrandom sequence, following a "shifting-X" pattern designed to avoid revisiting the vicinity of recently stimulated sites (Shepherd *et al.*, 2003; Shepherd & Svoboda, 2005). A modified version of Ephus software (Ephus, available at https://openwiki.janelia.org/) was used to control photostimulation protocols and acquire photostimulation data.

As indicated in Figure 1, a dual camera port was used to couple the Q-imaging CCD camera (Retiga 2000, Q-imaging Inc, Austin, TX) and the LSPS system to a MiCAM02 fast imaging system (SciMedia USA Ltd, Costa Mesa, CA) for voltage sensitive dye imaging. The VSD imaging computer (B) was independent from the computer (A), but its image acquisitions were triggered and synchronized with computer A through output TTL pulses from computer A. Upon triggering, optical recording of VSD signals was performed by the MiCAM02 system with a sampling rate of 2.2 ms per frame (frame resolution 88 (w) x 60 (h) pixels). The photostimulation and imaging systems were aligned and uncaging tests were visualized by exciting caged fluorescein dextran on a glass slide (Xu et al., 2010). Under the 4x objective, the laser beam formed uncaging spots, each approximating a Gaussian profile with the estimated full width at the half maximal fluorescence intensity of about 150 μm laterally at the focal plane; and the laser beam caused uncaging of fluorescent dextran at ~100 μm in depth. It is important to note that the physical laser excitation size in the glass slide does not directly translate into the effective spatial resolution of physiological uncaging in brain slices (see below). In comparison, under the 60x objective, the UV laser induced uncaging was focused to a smaller spot with the estimated full width at the half maximal intensity of about 2 μm. While photostimulation through the 60x objective is useful for exciting smaller numbers of neurons or possibly even single cell stimulation, our current work focused on both imaging and excitation through the 4x objective to map propagation of activity within local cortical circuits.

Electrophysiological recordings, photostimulation, and imaging of the slice preparations were done in a slice perfusion chamber mounted on a motorized stage of the microscope. Slices were visualized with an upright microscope (BW51X; Olympus, Tokyo, Japan) with infrared differential interference contrast optics. At low magnification (4x objective lens, 0.16 NA; UPlanApo; Olympus), laminar and cytoarchitectonic features of brain slices were visualized under infrared bright-field transillumination; and the slice images were acquired by the Q-imaging camera. Digitized images from the camera were used for guiding and registering photostimulation sites in brain slices. During experiments, simultaneous electrophysiological recordings (whole cell recordings, loose-seal patchings or local field potential recordings) were conducted to monitor laser stimulation and correlate VSD signals with the electrical activity. To perform patch recording, cells were visualized at high magnification (60x objective, 0.9 NA; LUMPlanFl/IR; Olympus). Neurons were patched with borosilicate electrodes and recorded at room temperature in the whole-cell or loose-seal mode. The patch pipettes (4-6 MΩ resistance) were filled with an internal solution containing 126 mM K-gluconate, 4 mM KCl, 10 mM HEPES, 4 mM ATP-Mg, 0.3 mM GTP-Na, 10 mM phosphocreatine (pH 7.2, 300 mOsm). The electrodes also contained 0.5-1% biocytin for cell labeling and morphological identification. Resting membrane potentials were measured immediately after electrodes broke into the cells following formation of a gigaohm seal, and current pulses were injected to examine each cell's basic electrophysiological properties. Data were acquired with a Multiclamp 700B amplifier (Molecular Devices, Sunnyvale, CA), data acquisition boards (models PCI MIO 16E-4 and 6713; National Instruments, Austin, TX), and Ephus software. Data were filtered at 2 kHz using a Bessel filter and digitized at 10 kHz and stored on a computer. Once stable whole-cell recordings were achieved with good access resistance (usually <20 MΩ), the microscope objective was switched from 60x to 4x for laser scanning photostimulation. The same low-power objective lens was used for delivering the UV flash stimuli.

Stock solution of MNI-caged-l-glutamate (4-methoxy-7-nitroindolinyl-caged l-glutamate, Tocris Bioscience, Ellisville, MO) was added to 20-25 ml of circulating ACSF for a concentration of 0.2 mM caged glutamate. After 5-6 hours of experimentation, the bath solution and MNI-glutamate was refreshed. Care was taken to ensure a constant fluid level in the chamber of ~ 2.0-2.5 mm above the slice to avoid small fluctuations in UV attenuation. For some experiments, the addition of 10 µM CNQX (6-Cyano-7-nitroquinoxaline-2,3-dione disodium, Tocris Bioscience) and 10 µM CPP (3-(2-Carboxypiperazin-4-yl)-propyl-1-phosphonic acid, Tocris Bioscience) in solutions were used to block ionotropic glutamate receptors. In addition, modified ACSF containing 0.2 mM Ca^{2+}, 4 mM Mg^{2+} was used to block synaptic transmission.

To prepare living brain slices, wild type C57/B6 mice (postnatal day 17–23) were deeply anesthetized with Nembutal (>100 mg/kg, i.p.), rapidly decapitated, and their brains removed. Visual cortical or hippocampal sections were cut 400 µm thick with a vibratome (VT1200S; Leica Systems, Germany) in sucrose-containing artificial cerebrospinal fluid (CSF) (in mM: 85 NaCl, 75 sucrose, 2.5 KCl, 25 glucose, 1.25 NaH_2PO_4, 4 $MgCl_2$, 0.5 $CaCl_2$, and 24 $NaHCO_3$). Slices were first incubated in sucrose-containing ACSF for 30 minutes to 1 hour at 32°C, and after the initial incubation period, transferred to recording ACSF (in mM: 126 NaCl, 2.5 KCl, 26 $NaHCO_3$, 2 $CaCl_2$, 2 $MgCl_2$, 1.25 NaH_2PO_4, and 10 glucose) for the dye staining at room temperature. The slices were stained for 1-2 hours in a staining chamber containing ACSF with 0.02 mg/ml of an oxonol dye, NK3630 (available from Nippon Kankoh-Shikiso Kenkyusho Co., Ltd., Japan), and then maintained in regular ACSF before use. The NK3630 dye has been characterized in previous studies and has its peak signal-to-noise ratio centered around 705 nm (Jin et al., 2002). Throughout the incubation, staining and recording, the slices were continuously bubbled with 95% O_2-5% CO_2.

2.2 LSPS system calibration and VSD imaging tests

The effective physiological resolution of photostimulation in our system was assessed by measuring neuronal excitation profiles, which quantify the spatial distribution of uncaging sites that produce action potentials in individually recorded neurons; similar approaches to assess the distribution of evoked neuronal excitability have been used by other groups (Shepherd *et al.*, 2003; Shepherd & Svoboda, 2005; Weiler *et al.*, 2008). Specifically, the spatial resolution of effective photostimulation, R, was quantitatively estimated as the mean distance between the soma and the spike-generating sites weighted by the number of spikes per site [i.e., R = Σ(r × n)/Σn, where for each site, r is the distance to the soma and n is the number of spikes]. Under our normal photostimulation conditions through the 4x objective (power level: 20–35 mW; pulse duration: 1-2 ms), the average R across excitatory neurons in primary visual cortex (V1) was about 90 µm across different V1 layers (Xu et al., 2010). This is illustrated in Figure 2A-B, as LSPS had a spatial resolution of 50-100 µm in evoking suprathreshold spikes from the recorded neuron in a V1 slice. Therefore, photostimulation in our experiments could provide spatially restricted neuronal activation, and offered a sufficient resolution for V1 laminar circuit mapping. However, under stronger photostimulation conditions (power level: 30-35 mW; pulse duration: 3 ms or above), the spatial resolution of photostimulation was lowered as spikes could be evoked from cells located 100-300 µm away from the stimulation sites. The stronger laser stimulation evoked neuronal spikes from the cells located far away from the photostimulation sites possibly either through direct activation of distant dendrites or through strong synaptic drive

(Dantzker & Callaway, 2000; Weiler *et al.*, 2008). Hence, in hippocampal circuit mapping experiments that we have conducted, strong laser stimulation was used to further assess trans-synaptic spread of activity.

During experiments, a 705 nm light trans-illuminated brain slices, and voltage-dependent changes in the light absorbance of the dye were captured by the MiCAM02 camera (Figure 1). Under the 4x objective, the imaging field covered the area of 1.28 x 1.07 mm2 with a spatial resolution of 14.6 x 17.9 μm2/pixel. With the 60x objective, the imaging field covered the area of 84.5 x 70.8 μm2 with a resolution of 0.96 x 1.18 μm2/pixel. The trials were obtained every 8 seconds and the recording periods were 1000 frames for each trial. VSD images were smoothed by convolving images with a Gaussian spatial filter (kernel size: 3x3 pixels; δ size: 1x1 pixel) and a Gaussian temporal filter (kernel size: 3 frames; δ size: 1 frame). VSD signals were originally measured by the percent change in pixel light intensity [$\Delta I/I$ %; the % change in the intensity (ΔI) at each pixel relative to the initial intensity (I)]. In addition, signal amplitudes were expressed as standard deviations (SD) above the mean baseline signal for display and quantification.

Because photostimulation and VSD imaging are combined, separation of the laser excitation and the VSD signal is important. Given the UV laser and the VSD absorption light have differing wavelengths (355 nm vs ~705 nm), the laser and its excitation artifact had been significantly reduced using a band-pass filter centered at 705 nm right before the imaging camera (See Figure 1). Furthermore, when using short laser pulses (i.e., 1-3 ms), the laser artifact signal only existed in the initial 2 image frames (2.2 ms per frame). Compared to the VSD signal reflecting neural activity (0.1-0.5%), the artifact signal was large, up to 2% change from baseline (Figure 3B1-B4), however did not interfere with true VSD signals, considering detectable VSD responses occurred approximately 5-6 frames after the laser onset.

Successful combination of VSD imaging with laser photostimulation was exemplified in Figure 2C and D through the 4x and 60x objectives, respectively. In Figure 2C, the image data were from a coronal slice of mouse primary visual cortex (V1) with photostimulation and imaging through the 4x objective. In response to the spatially restricted laser stimulation, the evoked neural activity reflected by VSDsignals was initiated at the stimulation site shortly after the laser onset, and gradually propagated and spread to other regions. As shown in Figure 2D, VSD imaging and photostimulation was also achieved through the 60X objective; the VSD response was the strongest at the stimulation location with weaker activation in the surroundings. In the present study, single-trial photostimulation-evoked VSD responses were sufficiently strong and could be discerned from background noise; hence no averaging over multiple trials was necessary.

2.3 Characterization of photostimulation-evoked VSD responses

In V1 imaging experiments, we characterized photostimulation-evoked VSD responses. The VSD signal results from the summed signal of neuronal ensembles; but the observed properties of photostimulation evoked VSD signals were closely related to membrane potential depolarization of individual neurons (Figure 3B1- B4). Spikes responded faster to photostimulation than VSD signals, as the average spike peak time in response to photostimulation was 11.8 ± 3 ms, and the average VSD signal peak time was 29.9 ± 6.3 ms (Xu et al., 2010). In these experiments, the average VSD response latency across different V1 layers was 15.4 ± 0.7 ms.

As exemplified in Figure 3A-E, the photostimulation-evoked VSD responses were mediated by glutamate and its receptors, as neuronal spiking and VSD responses to glutamate uncaging were essentially abolished by the ionotropic glutamate receptor antagonists (CPP and CNQX). There was no VSD signal without glutamate uncaging; laser flashes alone did not activate neurons or induce VSD responses. There was no detectable signal in brain slices without VSD staining in response to photostimulation, indicating that photostimulation-evoked VSD responses were not contaminated by activity-related tissue autofluorescence signals (Shibuki et al., 2003; Llano et al., 2009). Furthermore, reducing synaptic transmission from stimulated neurons using low Ca2+ and high Mg2+ ACSF solution restricted VSD changes to the region near the stimulation site. This indicates that most activity far away from the stimulation site reflected synaptic spread of activity to postsynaptic neurons rather than activity in the axons and distant dendrites of directly stimulated cells (Figure 3F-H). This is similar to the result observed in TTX, which blocks both synaptic spread and conduction of activity with the axons of stimulated cells.

3. Visual cortical circuit mapping

Compared to previous studies of V1 circuits that used VSD imaging with electrical stimulation or puffed glutamate at different cortical locations (Nelson & Katz, 1995; Yuste *et al.*, 1997), our new technique allows us to evaluate laminar propagation of evoked excitation and probe functional connectivity of mouse V1 laminar circuits, with a much improved precision and speed.

The new technique has been used to map activity propagation and layer-specific output patterns in V1 local circuits. Under the stimulation conditions used, LSPS (1ms, 20-35 mW) offered spatially restricted neuronal activation in a specific cortical layer so that we were able to map direct projections from the stimulated layer to its targeted layer(s) by VSD imaging of evoked activation. That is, photostimulation-evoked action potentials were restricted to neurons with cell bodies at or close to the stimulation site; activity then propagated through the axons of the stimulated neurons and generated postsynaptic responses in the neurons that were connected to the stimulated cells. The measured VSD signals reflected the combined contributions of these sources, but responses distant from the stimulation site were dominated by postsynaptic changes, as evidenced by control experiments in which synaptic transmission was blocked by using low Ca2+ and high Mg2+ ACSF (see above). Figure 4A, B and C show VSD image frames in response to laser photostimulation at cortical layers 2/3, 4 or 5 in a V1 coronal slice, respectively, while Figure 4D shows VSD image frames in response to electrical stimulation at V1 layer 4. In comparison, layer 4 photostimulation was effective as electrical stimulation in evoking population neuronal responses, but its activation was more restricted and specific (compare Figure 4B6 and Figure 4D6). Unlike electrical stimulation, a significant advantage of photostimulation is such that uncaged glutamate does not activate passing axon fibers (Xu et al., 2010), thus ensuring spatial specificity of stimulation and avoiding antidromic presynaptic activation. During photostimulation and VSD imaging experiments, stimulation in V1 cortical layers initiated excitation which resulted in VSD signals first localized to the stimulation site at around 10-20 ms after laser exposure; excitation then propagated to functionally connected cortical regions. For layer 2/3 stimulation, the activation in layer 2/3 was mostly localized in layer 2/3, however, relatively small but clear activation propagated from layer 2/3 to layer 5, bypassing most of layer 4 (Figure 4A1-A6). There was essentially

no excitation from layer 2/3 propagating to layer 6. Stimulation in layer 4 caused excitatory activity to spread vertically to layers 2/3 and 5, but with little excitation in layer 6 (Figure 4B1-B6). Strong activation in layers 2/3 and 5 due to layer 4 stimulation indicates these layers receive strong direct projections from layer 4. Layer 5 stimulation resulted in distinct foci of activation in layer 2/3 (Figure 4C1-C6), and some activation spread into layers 6 and 4. Layer 6 stimulation resulted in mostly localized responses, but some activation could spread into upper layers with stronger phostimulation.

This new technique has also been used to investigate spatiotemporal patterns of activity in tangential slices of visual cortex. As shown in Figure 5, photostimulation evoked VSD responses propagated largely in horizontal directions, and their response patterns evolved into extended clusters of distinct activation domains. The pattern of population activity reflected anatomical horizontal connections to the stimulation sites. There were spatial shifts in the distribution of activation domains that resulted from different photostimulation sites. The clustered activation domains seen in the tangential slices were similar to that found in ferret visual cortex, but at a much finer scale. This is perhaps due to the spatially restricted neuronal activation by photostimulation instead of electrical stimulation used in previous studies (Tucker & Katz, 2003).

In addition, as LSPS activates many different sites with very short time intervals (e.g., see Figure 2A-B), our technique enables rapid mapping of neuronal circuitry by patterned photostimulation and VSD imaging of multiple V1 locations. This approach is much faster and more efficient than mapping with electrical stimulation at different locations, considering the time required for proper electrode placement on the order of minutes. As illustrated in Figure 6, an array of 4 x 4 photostimulation sites (cyan stars, in Figure 6A1) covered the V1 cortical area at different laminar locations. During this experiment, the laser stimulation was a 1ms laser flash at 35 mW with a stimulation interval of 8 seconds; the whole duration of VSD mapping for all 16 locations only took 128 seconds. Figure 6C1-C16 shows the overall laminar profile of photostimulation-evoked VSD responses by presenting peak activation frames at each of the 16 stimulation sites covering V1 from cortical layer 2/3 to layer 6. LSPS resulted in laminar specific patterns of excitatory output detected by VSD imaging.

Based upon high-resolution mapping data, we can quantify patterns of evoked activation in individual cortical layers to analyze interlaminar functional connectivity of local V1 circuits. Provided that VSD activation outside the stimulation site mostly reflects synaptic spread of activity to postsynaptic neurons rather than activity in the axons and distant dendrites of directly stimulated cells in the photostimulated layer, we can construct a functional connectivity diagram for mouse V1 local circuits based upon quantitative analysis of propagation activity from multiple laminar locations (Xu et al., 2010). Moreover, our data allows for quantification of functional interlaminar projection strength. Specifically, based upon the excitation profile data, it is estimated that each photostimulation activated approximately 250 neurons within ~90 μm of the laser uncaging center, as N spiking = ρ Vexc , where the number of spiking neurons, N spiking is determined by the mouse cortical neuronal density, ρ and the volume of excited neurons, Vexc [the product of photostimulation-evoked spiking area ($\pi R2$) and the photostimulation axial penetration depth in the brain slices (~ 50-100 um; an average of 75 um is used for calculation)]. The neuronal density in mouse visual cortical layers 2/3, 4, 5 and 6 has been previously quantified (Schuz & Palm, 1989). Therefore, the average number of spiking neurons (N spiking) per photostimulation under normal experimental conditions can be calculated. As

the number of presynaptic spiking neurons by each photostimulation is known, the projection strength of these neurons could be quantitatively defined with the measurement of evoked activation by VSD imaging in their functionally connected regions (Olivas et al., submitted). Taken together, our new technique yields precise and quantitative mapping data for functional circuit analysis.

4. Hippocampal circuit mapping

We have extended our technique to investigation of spatiotemporal dynamics of hippocampal circuit activity. We are particularly interested in understanding whether or how a restricted population of dentate neurons (e.g., granule cells) can engage the entire trisynaptic circuit. We photo-stimulated different locations in the dentate gyrus (DG) such as the molecular layer, the granule cell layer and the hilus, and monitored how evoked responses initiated and propagated throughout the hippocampal circuitry.

For the illustration purpose, we present example data of stimulation in the DG molecular layer as shown in Figure 7. In this experiment, restricted photostimulation occurred in the superior blade of DG molecular layer (indicated by small cyan star in Figure 7A). This uncaging mimicked the perforant pathway stimulation, and induced serial excitatory propagation in DG, CA3 and CA1 (Figure 7C). As shown in Figure 7B, we simultaneously monitored optical recordings with field potential recordings at CA3, and the optical signal from the ROI in CA3 correlated well with electrical activity reflected by the field potential at that location. Our technique clearly revealed the information flow along the trisynaptic circuitry in hippocampus. After a short delay of the photostimulation in the molecular layer, the VSD response first initiated in the granule cell layer, traversed through polymorphic layer (hilus), and reached CA3 and then CA1 (Figure 7C). This stimulation caused long-lasting excitation in DG, CA3 and CA1. The excitation in CA3 and CA1 was extensive; the amplitudes of the optical signals in pyramidal cell layer were stronger than those in stratum radiatum or stratum oriens. In contrast, clearly the CA2 region did not have strong excitation (see the white arrows in Figure 7C), which supports evidence that CA2 lacks of the granule cell input (Swanson et al., 1978; Nakagami et al., 1997). The data illustrate a localized DG neuronal population effectively engaged in the excitatory flow of information throughout DG and the hippocampus proper collectively, thus providing a comprehensive perspective of the functional circuit organization and dynamics of the hippocampal pathway.

5. Further technical development

As an alternative method of photostimulation via glutamate uncaging, optogenetical approaches can be used to make neurons directly photoactivated via channelrhodopsin-2 (ChR2) (Boyden et al., 2005; Zhang et al., 2006; Gradinaru et al., 2010). ChR2 is a light-sensitive nonselective cation channel isolated from the green alga *Chlamydomonas reinhardtii*, which can transduce light energy into neural activity when expressed in neurons (Boyden et al., 2005). Therefore, in our new technique, glutamate uncaging can be replaced with photoactivation via channelrhodopsin or other genetically encoded photosensitive molecules expressed in cortical neurons (Boyden *et al.*, 2005; Kuhlman & Huang, 2008). Genetically encoded ChR2 can also enhance the ability of photostimulation in targeting define cell types, as glutamate uncaging indiscriminately stimulates all neurons expressing

glutamate receptors. Figure 8 exemplifies our ability of VSD imaging with ChR2 photoactivation. We take advantage of the transgenic mouse line expressing ChR2 in subsets of excitatory pyramidal neurons under the control of the Thy1 promoter (Figure 8A), and have mapped local cortical circuitry using the blue laser photostimulation (475 nm laser, 2mW, 1ms) without the aid of caged glutamate. As shown in Figure 8 C, compared to photostimulation via glutamate uncaging, ChR2 activation was much faster, with an imaging response latency of less than 1 image frame (2.2 ms). In addition, the population neuronal activity induced by ChR2 photoactivation was quite strong and the activity propagation pattern was similar to that evoked by glutamate uncaging (Figure 8B and C). A caveat is that ChR2 activation has an issue of spatial precision of photostimulation as action potentials can be elicited by photostimulating the soma and dendrites as well as the axon (Petreanu et al., 2007). Regardless, this new development makes it possible to target not only specific cortical regions but also specific subset of neurons within their participating circuits through laser scanning photostimulation.

Our technique can be generally extended to other fast dye imaging. For example, when calcium indicators are used, LSPS can be combined with calcium imaging. As the optical signals of VSD and calcium indicators differentially report subthreshold postsynaptic potentials and local action potential firing, and as simultaneous VSD and calcium imaging using epifluorescence optics has been reported to measure the spatiotemporal dynamics of activity in cortical circuits in vitro and in vivo (Berger et al., 2007), we plan to combine both VSD and calcium imaging with laser scanning photostimulation, which will allow us to monitor both the synaptic drive and the spiking activity of a given circuit location at the same time. Compared to VSD measurements, the drawbacks of calcium measurements include the concern that some cells or cell types that produce action potentials may not produce measurable Ca2+ transients, and the inability of calcium dyes to detect inhibitory synaptic activity (Knopfel *et al.*, 2006).

Although we have successfully used synthetic voltage-sensitive dyes in our technical implementation, the conventional dyes have certain limitations such as non-specificity of cell staining and side effects including toxicity and dye interference with neuronal membrane potentials and excitability (Mennerick et al., 2010). However, emerging optogenetics methods have started to overcome the problems of the conventional dyes by developing genetically encoded sensors and expressing such sensors in defined cell populations in vivo, thus avoiding background noise and enabling a rigorous assignment of optical response signals to specific cellular sources (Akemann et al., 2010). Clearly, this is an important consideration for our future improvement.

6. Discussion and conclusions

As described in this chapter, we have developed a new photostimulation-based technique through the integration of VSD imaging and LSPS for high precision and rapid mapping of in vitro functional circuits at the neuronal population level. The incorporation of LSPS has greatly enhanced the ability of assessment of evoked network activity by fast VSD imaging. The "dream-team" methods of stimulation and imaging make this new technique quite effective in mapping neuronal circuit dynamics and organization.

Photostimulation based mapping techniques have been widely applied for analyzing cortical circuits. LSPS combined with whole cell recordings is an effective method for mapping local circuit inputs to single neurons, as the simultaneous recording from a

postsynaptic neuron with photostimulation of clusters of presynaptic neurons at many different locations provides quantitative measures of spatial distribution of excitatory and inhibitory inputs impinging onto single recorded neurons (Callaway & Katz, 1993; Schubert *et al.*, 2003; Shepherd & Svoboda, 2005; Xu & Callaway, 2009). LSPS has also been combined two-photon calcium imaging to generate detailed functional maps of inputs to individual cells with single-cell and three-dimensional precision (Nikolenko *et al.*, 2007). Different from the aforementioned approaches, our newly developed technique is intended to assess circuit activation and network connectivity at the neuronal population level through fast VSD imaging and photostimulation. As our technique is often performed with simultaneous electrophysiological recordings of single neurons, the method is readily combined with whole-cell patch-clamp measurements of electrical signals in brain slices so that local cortical circuits can be examined in the same brain slice at both single cell and population levels. Note that laser photostimulation has been combined with intrinsic flavoprotein auto fluorescence imaging to map long range neural connections in the thalamocortical slice (Llano et al., 2009), but the imaging of intrinsic signals generally lacks the temporal and spatial resolution required for studies of local circuit connections and dynamics.

Our technique can have important applications in the field of cortical circuitry as demonstrated in our studies of mouse V1 and hippocampal circuits. As the mouse is an important model system for cortical circuit studies and mouse V1 circuits are less well understood, we imaged and probed V1 with spatially restricted photostimulation, and mapped interlaminar functional connectivity and circuit dynamics. This technique enabled direct visualization of interlaminar functional connections in V1 circuits at a previously unattainable precision (Burkhalter, 1989; Yuste et al., 1997; Callaway, 1998). Overall, our mouse V1 data fit with and extend previous anatomical and physiological observations of laminar patterns of axonal projections in rodent V1 local circuits (Burkhalter, 1989; Yuste et al., 1997), and is generally consistent with proposed V1 laminar operational schemes (Gilbert, 1983; Callaway, 1998). Although our V1 results are as expected from known anatomy and connectivity in the rodent visual cortex (Burkhalter, 1989; Yuste et al., 1997), this method would be valuable for assaying brain areas, species, or genetically modified mouse lines in which these data are not presently available. In addition, the application of this technique to the hippocampal circuitry mapping further validated its technical power and effectiveness. The circuit dynamics and functional connection in the hippocampal circuitry were mapped through spatially restricted activation of a subset of DG neuronal population. With strong photostimulation, we were able to examine the perspective of the polysynaptic spread of activity in detail.

As this is all-optical technique to image and evoke circuit activity, our new method can be further developed as a methodology for identification and monitoring of real-time responses in vitro (e.g., cell cultures and slice preparations) to drugs, therapeutic or genetic interventions. The immediate application can be extended for fast and effective screening of circuit alterations in transgenic animal models recapitulating specific neurological diseases at a large scale.
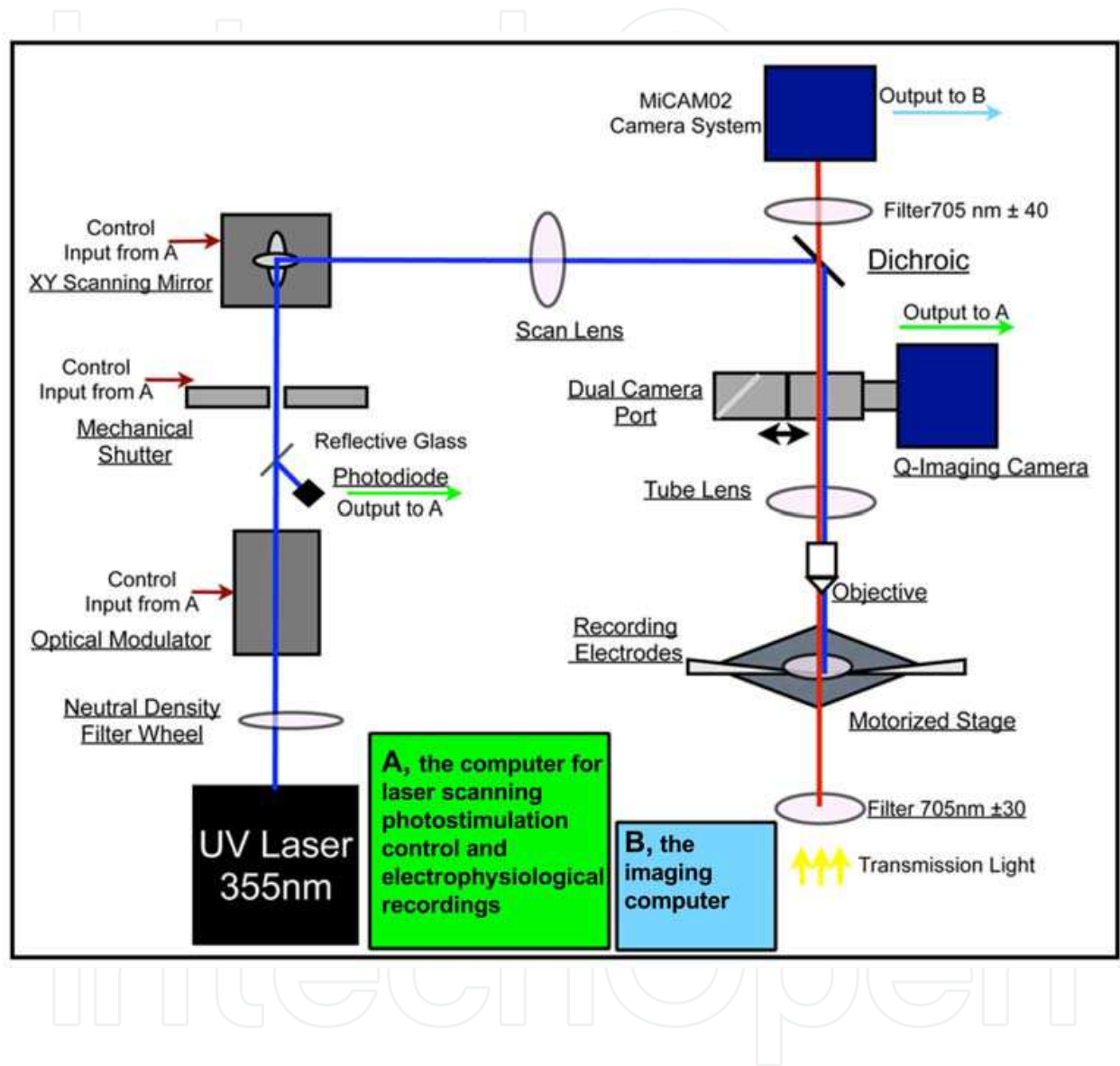
7. Acknowledgements

Fig. 1. **The general system design for combining laser scanning photostimulation (LSPS) with voltage sensitive dye (VSD) imaging.** The diagram shows the whole system consisting of laser scanning photostimulation, VSD imaging, and electrophysiological recording systems. This figure was modified from Xu et al. (2010) with permission of the American Physiological Society.
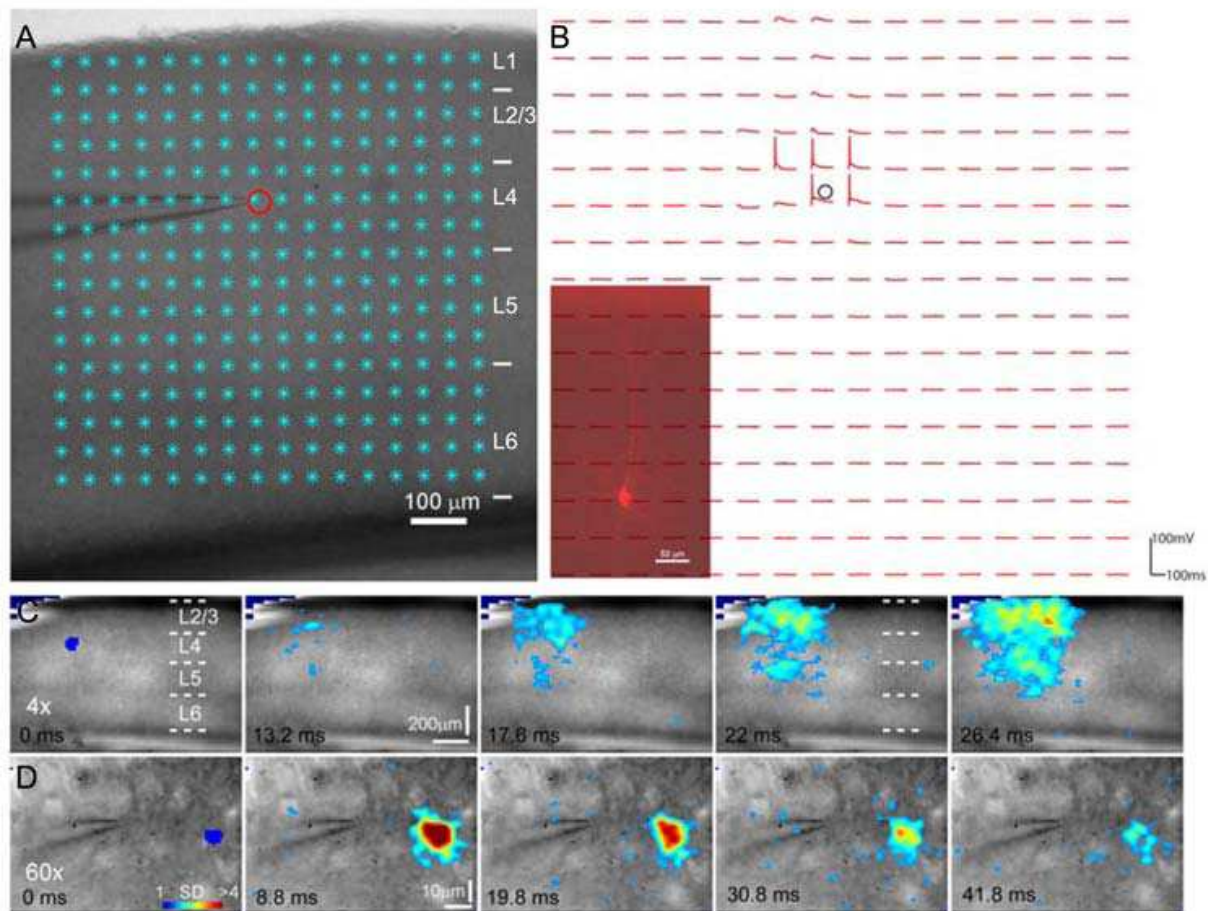
Fig. 2. **Physiological calibration of the LSPS system and example tests for combining photostimulation with VSD imaging.** A shows a mouse coronal V1 cortical slice image with the superimposed photostimulation sites (16 x 16 cyan stars, spaced at 50 μm x 50 μm) across cortical layers 1, 2, 3, 5 and 6 (i.e., L1-L6). The glass electrode was recording from an excitatory pyramidal neuron (with its morphology shown in the inset in B), with its location indicated by a small red circle. B shows the traces of membrane potential depolarization of the recorded neuron at the current clamp mode in response to LSPS (1ms, 30 mW, interstimulus interval, 400 ms) at the locations shown in A. Although subthreshold responses are seen at many locations, suprathreshold spikes only occur around the perisomatic area of the recorded neuron (indicated by the small black circle). C and D are sequences of VSD image frames in response to photostimulation through 4x and 60x objectives, respectively. Laser stimulation (32 mW) was 1 ms and 100 μs for C and D, respectively. The site of photostimulation can be identified by the laser excitation artifact in the initial frames of the sequences. Time progresses from left to right, and VSD signal amplitudes expressed as standard deviations (SD) above the mean baseline signal are color coded. Warmer colors indicate greater excitation. The map pixels with amplitudes ≥ 1 SD are plotted. Note that the CCD camera images have a slightly different aspect ratio. Under the 4x objective, the camera covers an area of 1.28 (w) x 1.07 (h) mm2 with a spatial resolution of 14.6 (w) x 17.9 (h) μm/pixel. The following figures use the same conventions.
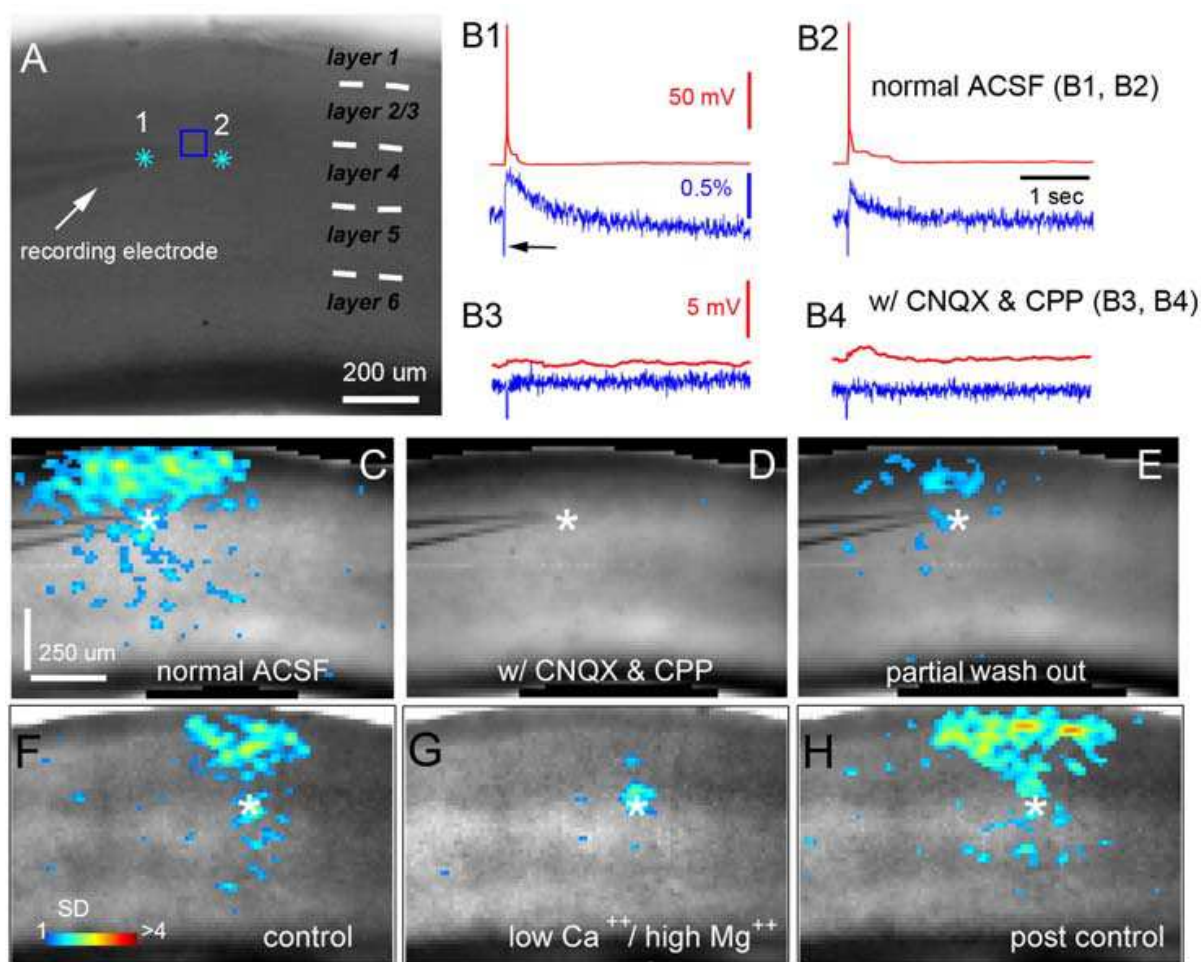
Fig. 3. **Characterization of photostimulation-evoked VSD responses.** A shows a gray scale image of V1 slice stained with NK3630, photostimulated (laser: 1 ms, 35 mW) at two sites (indicated by cyan stars) close to the recording electrode placed at the boundary of layers 3 and 4. The recorded neuron was identified as an excitatory pyramidal neuron. B1 and B2 are data traces of simultaneous whole-cell recording and VSD imaging in response to photostimulation at sites of 1 and 2 in normal artificial cerebrospinal fluid (ACSF), respectively. Red traces represent membrane potentials of the recorded neuron, and blue traces represent VSD signals that were measured from the region of interest (ROI) - marked by a blue square around the electrode tip shown in A. The black arrow in B1 points to the artifact signal of laser excitation in the VSD signal trace. B3 and B4 show data traces of simultaneous whole-cell recording and VSD imaging in response to photostimulation at the same sites as B1 and B2 but in ACSF with 10 μM CNQX and 10 μM CPP. C, D and E show VSD image frames of peak activation after glutamate uncaging at site 1 (indicated by the white star) before, after bath application and after wash out of CNQX and CPP, respectively. VSD signal amplitudes expressed as standard deviations (SD) above the mean baseline signal are color coded. F-H are peak activation frames of a different V1 slice in response to laser photostimulation in a layer 4 site (indicated by the white star; laser: 1ms, 35 mW) with perfusion of normal ACSF (control), low Ca2+ and high Mg2+ ACSF (containing 0.2 mM Ca2+, 4 mM Mg2+) and post-control normal ACSF, respectively. The data illustrate that most VSD responses outside the photostimulation site are predominantly postsynaptic responses which are blocked in the low Ca2+ and high Mg2+ solution. This figure is reproduced from Xu et al. (2010) with permission of the American Physiological Society.
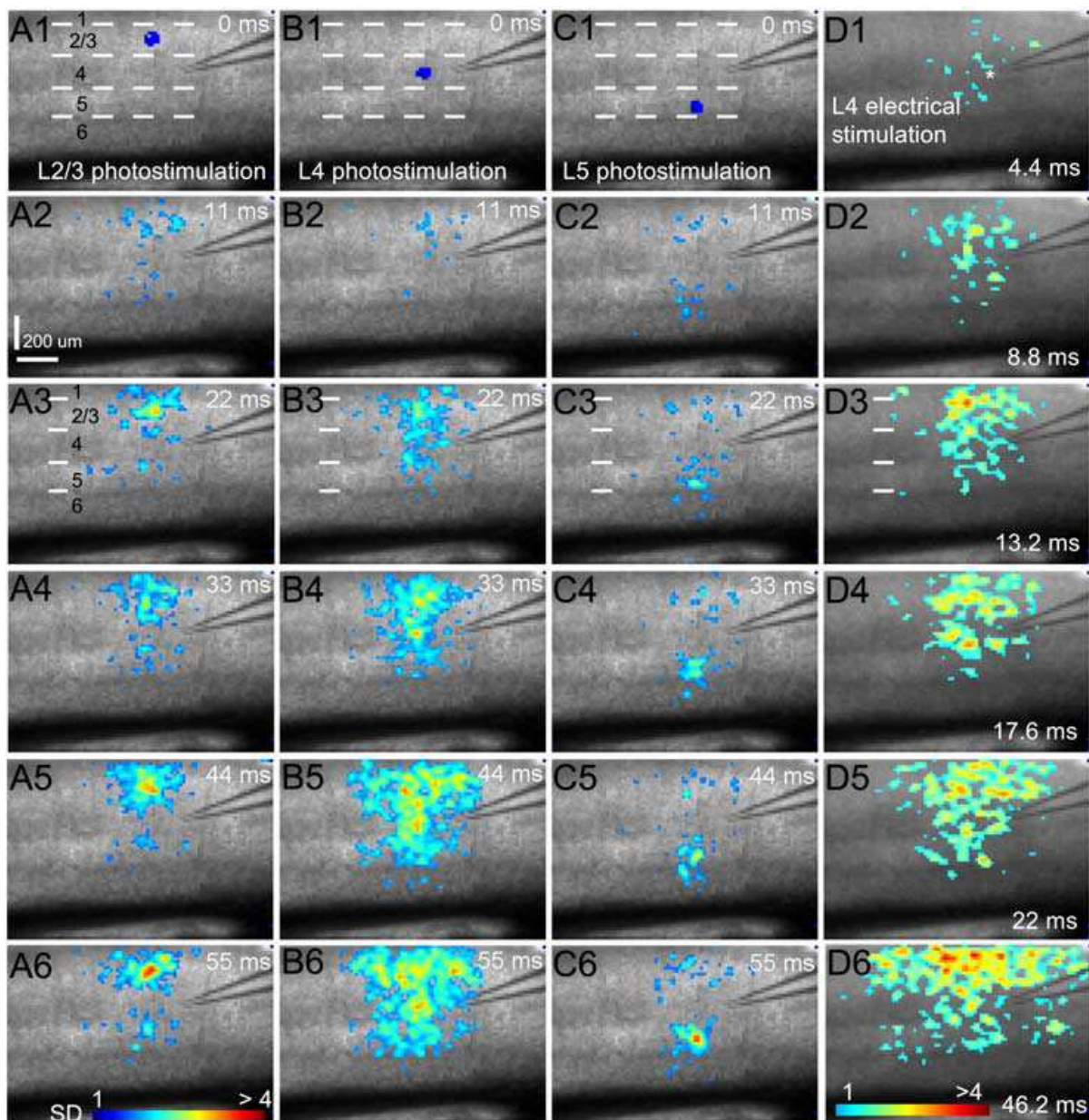
Fig. 4. **Spatially restricted neuronal activation via laser photostimulation enables high resolution mapping of interlaminar connections in mouse V1 local circuits.** A, B and C are sequences of VSD image frames in response to photostimulation (laser duration: 1ms; power: 32 mW) at cortical layers 2/3, 4 or 5 in a V1 coronal slice, respectively, while D shows VSD image frames in response to electrical stimulation (1ms, 50 µA current injection) through a microelectrode placed at V1 layer 4. VSD images were acquired at the rate of 2.2 ms/frame during the experiment, and are displayed at specific time points. Time progresses from top to bottom in the column, and color code is used to indicate VSD signal amplitudes expressed as standard deviations (SD) above the mean baseline. The map pixels with amplitudes ≥ 1 SD are plotted and included for further quantification. Warmer colors indicate greater excitation. The site of photostimulation can be identified by the laser excitation artifact (the blue spot) in the initial frames of the sequences. The short dashed white lines in the first image of A, B and C denote the laminar boundaries of V1 layers 1,

High Precision and Fast Functional Mapping
of Brain Circuitry through Laser Scanning Photostimulation and Fast Dye Imaging

127

2/3, 4, 5 and 6. VSD images in D1-D6 are color-coded differently from A-C. In D1, the white star indicates the tip of the glass pipette for electric stimulation. This figure is reproduced from Xu et al. (2010) with permission of the American Physiological Society.
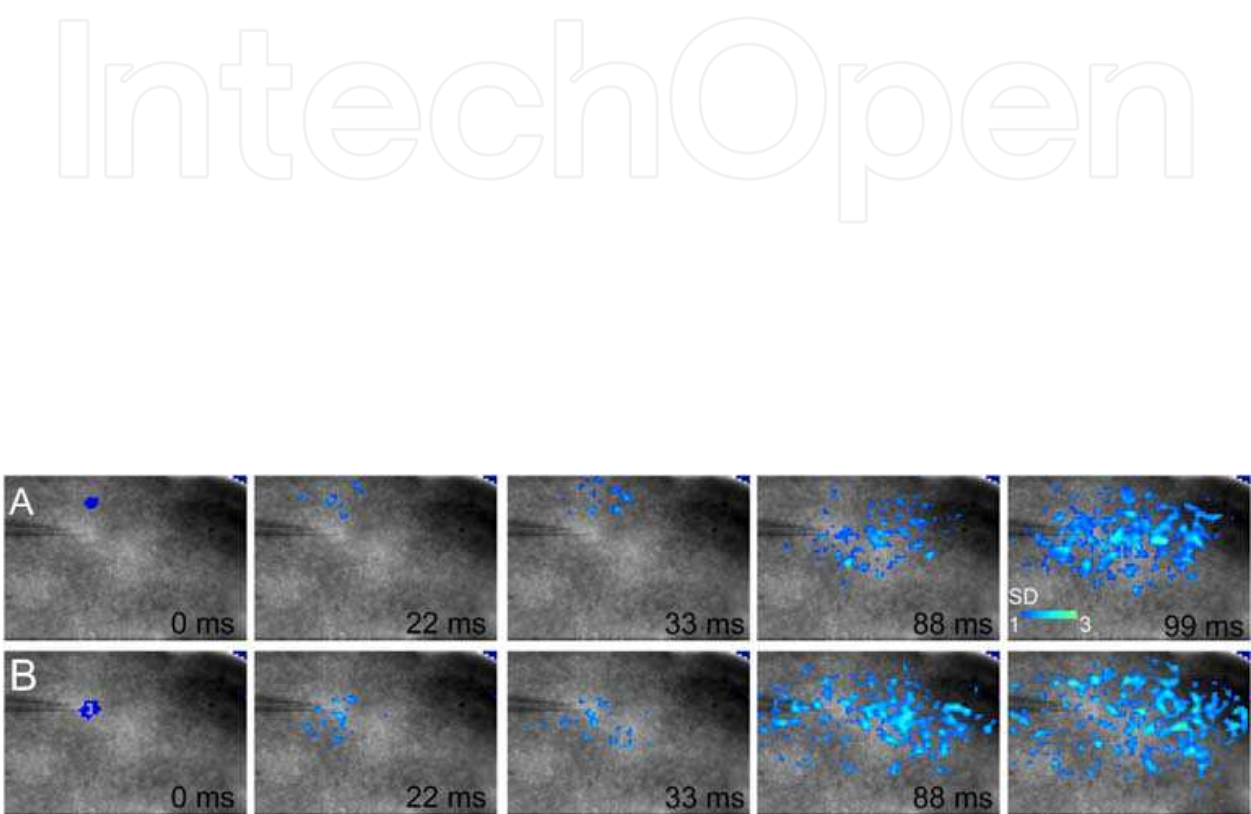

Fig. 5. **Photostimulation-evoked horizontal excitatory propagation in a V1 tangential slice.**
A and B are time frame series of VSD responses to photostimulation (30 mW, 2 ms) in two different locations, respectively, in the tangential slice of layer 2/3 in mouse visual cortex. The resulting patterns of VSD responses are characterized by an extended zone of activation domains from the stimulation site.
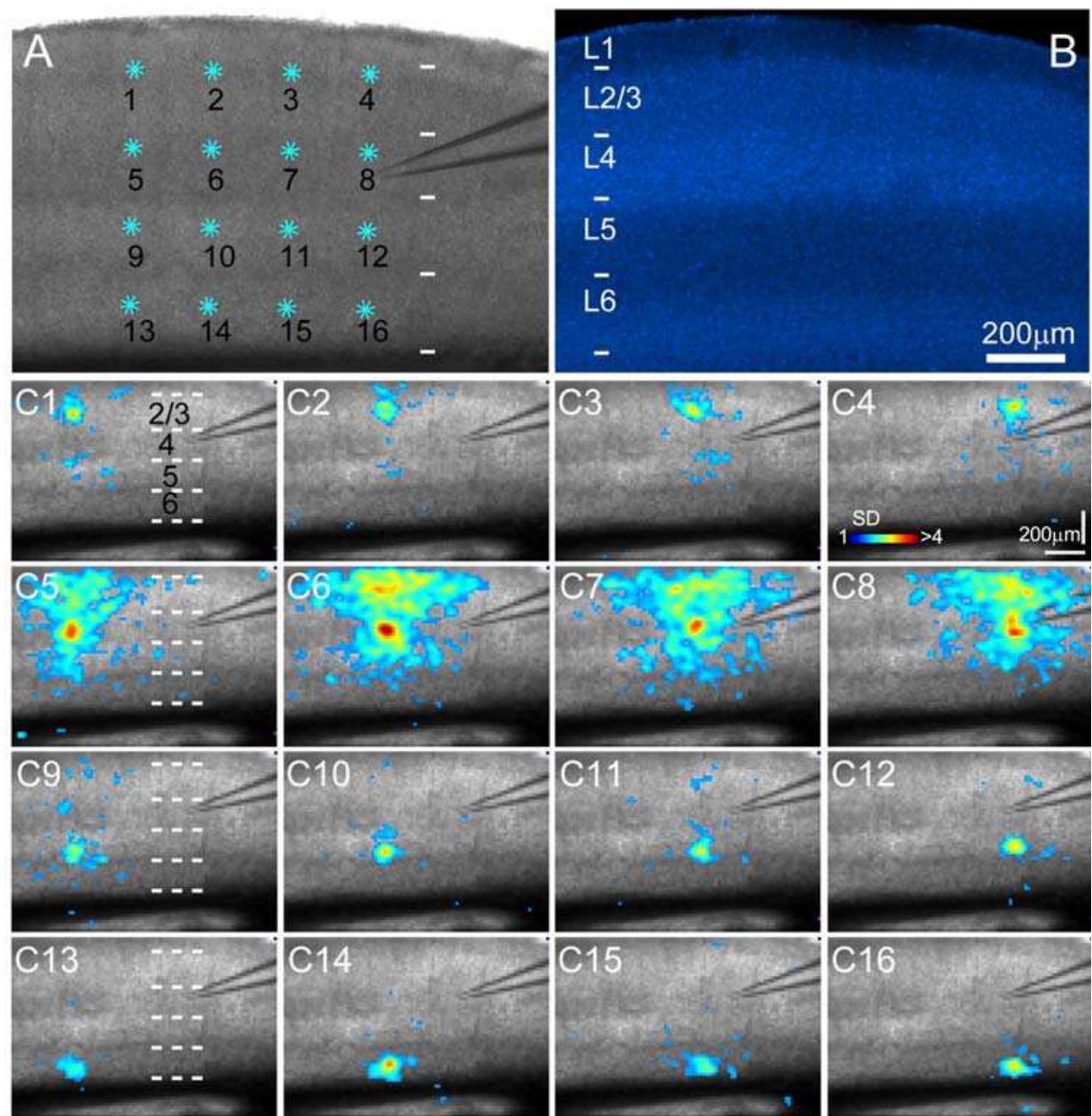
Fig. 6. **Rapid mapping of V1 local circuits through combination of VSD imaging and LSPS at multiple sites.** A shows the slice image with cyan stars indicating a 4x4 stimulus pattern covering V1 from cortical layer 2/3 to layer 6. The patch pipette was placed in the middle of layer 4 for extracellular electrical stimulation, while in most other experiments, a single pyramidal neuron was recorded during photostimulation and imaging for monitoring the effectiveness and spatial precision of laser photostimulation and correlating single-cell activity with the VSD imaged population response. B shows the DAPI-stained image of the same V1 slice as in A for laminar boundary designation. The short white lines in A, B, and C1, C5, C9 and C13 denote the laminar boundaries of layers 1, 2/3, 4, 5 and 6. C1-C16 show peak activation frames of the VSD map sequences corresponding to the 16 stimulation sites indicated in A.
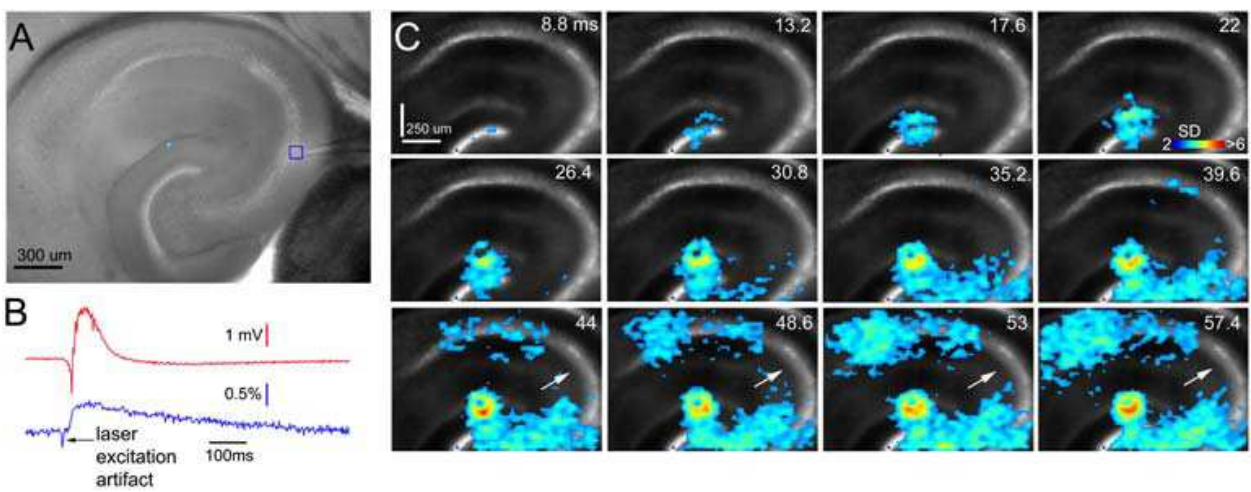
Fig. 7. **Hippocampal circuit mapping.** A shows a gray scale image of the hippocampus slice with the photostimulation site marked by a cyan star (in DG) and a blue square marking the ROI around the electrode tip in CA3. The data traces of the local field potential (in red) and the VSD signal (in blue) of the ROI shown in A are aligned in B to compare their temporal relationship. The VSD signal scale is in the percent change in light intensity [$\Delta I/I$ %]. C shows time frame series of the VSD response after photostimulation, and demonstrates a clear excitation flow through the hippocampal trisynaptic pathway. The white arrows in C point to the CA2 region which has little activation.
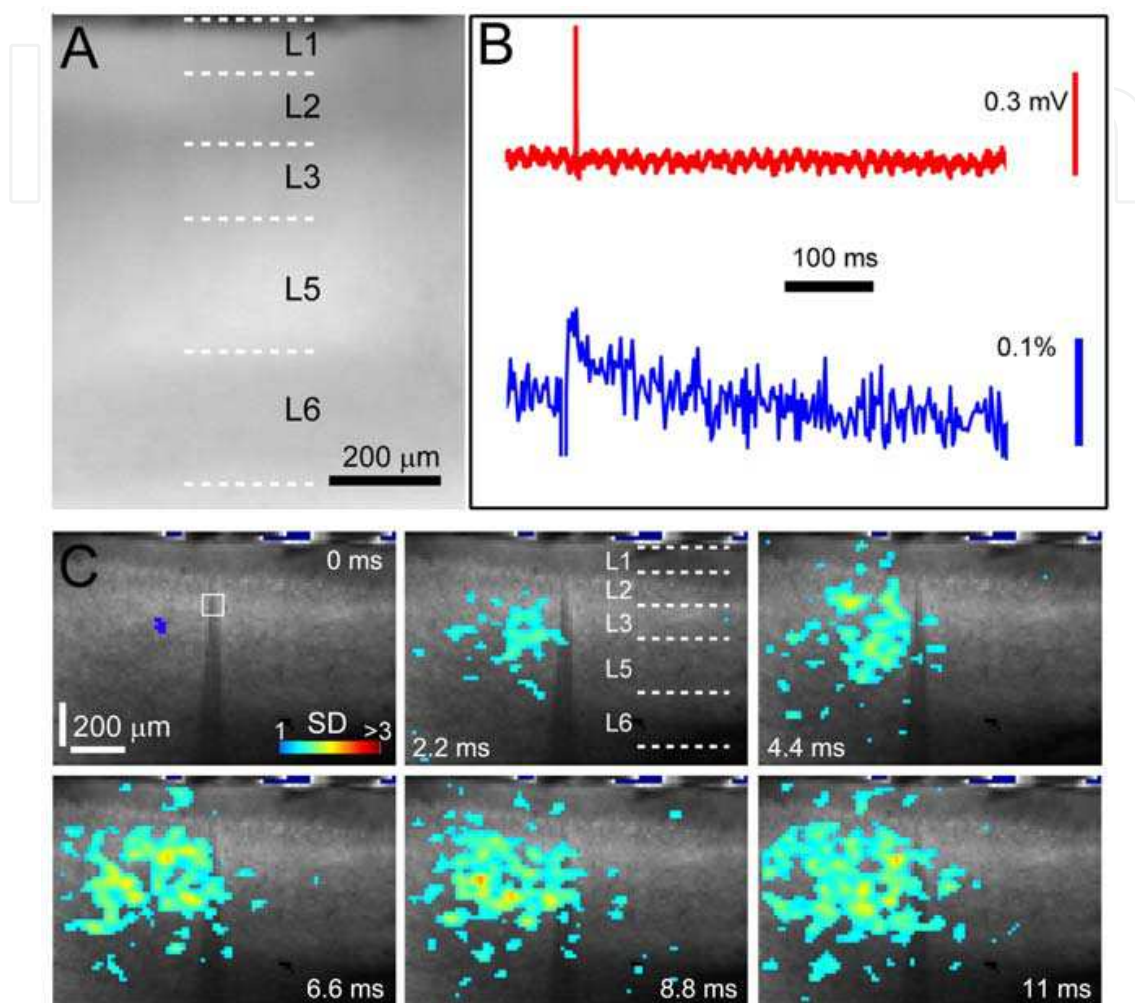
Fig. 8. **VSD imaging with channelrhodopsin-2 (ChR2) photoactivation.** A shows a yellow fluorescent proteins (YFP) fluorescent image of a medial prefrontal cortical slice from the transgenic mouse line expressing YFP- fused ChR2 mostly in subsets of excitatory pyramidal neurons under the control of the Thy1 promoter. This mouse line has relatively weak ChR2 in cortical layers 2 and 6, as reflected by the YFP fluorescence level. Note that medial prefrontal cortex lacks a granular layer 4 as seen in primary sensory cortices such as V1. B shows the aligned data traces of the local field potential (in red) and the VSD signal (in blue) of the ROI shown in C to compare their temporal relationship. The VSD signal scale is in the percent change in light intensity [$\Delta I/I$ %]. C shows time frame series of the VSD response to blue laser photostimulation (475 nm, 2 mW, 1 ms) in cortical layer 3 of the coronal slice, with both vertical and horizontal activity propagation.

8. References

Airan RD, Meltzer LA, Roy M, Gong Y, Chen H & Deisseroth K. (2007). High-speed imaging reveals neurophysiological links to behavior in an animal model of depression. *Science* 317, 819-823.

Akemann W, Mutoh H, Perron A, Rossier J & Knopfel T. (2010). Imaging brain electric signals with genetically targeted voltage-sensitive fluorescent proteins. *Nat Methods* 7, 643-649.

Ang CW, Carlson GC & Coulter DA. (2006). Massive and specific dysregulation of direct cortical input to the hippocampus in temporal lobe epilepsy. *J Neurosci* 26, 11850-11856.

Berger T, Borgdorff A, Crochet S, Neubauer FB, Lefort S, Fauvet B, Ferezou I, Carleton A, Luscher HR & Petersen CC. (2007). Combined voltage and calcium epifluorescence imaging in vitro and in vivo reveals subthreshold and suprathreshold dynamics of mouse barrel cortex. *J Neurophysiol* 97, 3751-3762.

Boyden ES, Zhang F, Bamberg E, Nagel G & Deisseroth K. (2005). Millisecond-timescale, genetically targeted optical control of neural activity. *Nat Neurosci* 8, 1263-1268.

Burkhalter A. (1989). Intrinsic connections of rat primary visual cortex: laminar organization of axonal projections. *J Comp Neurol* 279, 171-186.

Callaway EM. (1998). Local circuits in primary visual cortex of the macaque monkey. *Annu Rev Neurosci* 21, 47-74.

Callaway EM & Katz LC. (1993). Photostimulation using caged glutamate reveals functional circuitry in living brain slices. *Proc Natl Acad Sci U S A* 90, 7661-7665.

Dantzker JL & Callaway EM. (2000). Laminar sources of synaptic input to cortical inhibitory interneurons and pyramidal neurons. *Nat Neurosci* 3, 701-707.

Gilbert CD. (1983). Microcircuitry of the visual cortex. *Annu Rev Neurosci* 6, 217-247.

Gradinaru V, Zhang F, Ramakrishnan C, Mattis J, Prakash R, Diester I, Goshen I, Thompson KR & Deisseroth K. (2010). Molecular and cellular approaches for diversifying and extending optogenetics. *Cell* 141, 154-165.

Grinvald A & Hildesheim R. (2004). VSDI: a new era in functional imaging of cortical dynamics. *Nature reviews* 5, 874-885.

Huang X, Troy WC, Yang Q, Ma H, Laing CR, Schiff SJ & Wu JY. (2004). Spiral waves in disinhibited mammalian neocortex. *J Neurosci* 24, 9897-9902.

Jin W, Zhang RJ & Wu JY. (2002). Voltage-sensitive dye imaging of population neuronal activity in cortical tissue. *J Neurosci Methods* 115, 13-27.

Kandel E. (1982). The origins of modern neuroscience. *Annu Rev Neurosci* 5, 299-303.

Knopfel T, Diez-Garcia J & Akemann W. (2006). Optical probing of neuronal circuit dynamics: genetically encoded versus classical fluorescent sensors. *Trends Neurosci* 29, 160-166.

Kuhlman SJ & Huang ZJ. (2008). High-resolution labeling and functional manipulation of specific neuron types in mouse brain by Cre-activated viral gene expression. *PLoS ONE* 3, e2005.

Llano DA, Theyel BB, Mallik AK, Sherman SM & Issa NP. (2009). Rapid and sensitive mapping of long-range connections in vitro using flavoprotein autofluorescence imaging combined with laser photostimulation. *J Neurophysiol* 101, 3325-3340.

Mennerick S, Chisari M, Shu HJ, Taylor A, Vasek M, Eisenman LN & Zorumski CF. (2010). Diverse voltage-sensitive dyes modulate GABAA receptor function. *J Neurosci* 30, 2871-2879.

Nakagami Y, Saito H & Matsuki N. (1997). Optical recording of trisynaptic pathway in rat hippocampal slices with a voltage-sensitive dye. *Neuroscience* 81, 1-8.

Nelson DA & Katz LC. (1995). Emergence of functional circuits in ferret visual cortex visualized by optical imaging. *Neuron* 15, 23-34.

Nikolenko V, Poskanzer KE & Yuste R. (2007). Two-photon photostimulation and imaging of neural circuits. *Nat Methods* 4, 943-950.

Petersen CC & Sakmann B. (2001). Functionally independent columns of rat somatosensory barrel cortex revealed with voltage-sensitive dye imaging. *J Neurosci* 21, 8435-8446.

Petreanu L, Huber D, Sobczyk A & Svoboda K. (2007). Channelrhodopsin-2-assisted circuit mapping of long-range callosal projections. *Nat Neurosci* 10, 663-668.

Petreanu L, Mao T, Sternson SM & Svoboda K. (2009). The subcellular organization of neocortical excitatory connections. *Nature* 457, 1142-1145.

Schubert D, Kotter R, Zilles K, Luhmann HJ & Staiger JF. (2003). Cell type-specific circuits of cortical layer IV spiny neurons. *J Neurosci* 23, 2961-2970.

Schuz A & Palm G. (1989). Density of neurons and synapses in the cerebral cortex of the mouse. *J Comp Neurol* 286, 442-455.

Shepherd GM, Pologruto TA & Svoboda K. (2003). Circuit analysis of experience-dependent plasticity in the developing rat barrel cortex. *Neuron* 38, 277-289.

Shepherd GM & Svoboda K. (2005). Laminar and columnar organization of ascending excitatory projections to layer 2/3 pyramidal neurons in rat barrel cortex. *J Neurosci* 25, 5670-5679.

Shibuki K, Hishida R, Murakami H, Kudoh M, Kawaguchi T, Watanabe M, Watanabe S, Kouuchi T & Tanaka R. (2003). Dynamic imaging of somatosensory cortical activity in the rat visualized by flavoprotein autofluorescence. *J Physiol* 549, 919-927.

Swanson LW, Wyss JM & Cowan WM. (1978). An autoradiographic study of the organization of intrahippocampal association pathways in the rat. *J Comp Neurol* 181, 681-715.

Tucker TR & Katz LC. (2003). Spatiotemporal patterns of excitation and inhibition evoked by the horizontal network in layer 2/3 of ferret visual cortex. *J Neurophysiol* 89, 488-500.

Weiler N, Wood L, Yu J, Solla SA & Shepherd GM. (2008). Top-down laminar organization of the excitatory network in motor cortex. *Nat Neurosci* 11, 360-366.

Xu X & Callaway EM. (2009). Laminar specificity of functional input to distinct types of inhibitory cortical neurons. *J Neurosci* 29, 70-85.

Xu X, Olivas ND, Levi R, Ikrar T & Nenadic Z. (2010). High precision and fast functional mapping of cortical circuitry through a combination of voltage sensitive dye imaging and laser scanning photostimulation. J Neurophysiol 103, 2301–2312.

Yuste R, Tank DW & Kleinfeld D. (1997). Functional study of the rat cortical microcircuitry with voltage-sensitive dye imaging of neocortical slices. *Cereb Cortex* 7, 546-558.

Zhang F, Wang LP, Boyden ES & Deisseroth K. (2006). Channelrhodopsin-2 and optical control of excitable cells. *Nat Methods* 3, 785-792.

Laser Scanning, Theory and Applications
Edited by Prof. Chau-Chang Wang

Ever since the invention of laser by Schawlow and Townes in 1958, various innovative ideas of laser-based applications emerge very year. At the same time, scientists and engineers keep on improving laser's power density, size, and cost which patch up the gap between theories and implementations. More importantly, our everyday life is changed and influenced by lasers even though we may not be fully aware of its existence. For example, it is there in cross-continent phone calls, price tag scanning in supermarkets, pointers in the classrooms, printers in the offices, accurate metal cutting in machine shops, etc. In this volume, we focus the recent developments related to laser scanning, a very powerful technique used in features detection and measurement. We invited researchers who do fundamental works in laser scanning theories or apply the principles of laser scanning to tackle problems encountered in medicine, geodesic survey, biology and archaeology. Twenty-eight chapters contributed by authors around the world to constitute this comprehensive book.

How to reference

In order to correctly reference this scholarly work, feel free to copy and paste the following:

Xiangmin Xu (2011). High Precision and Fast Functional Mapping of Brain Circuitry through Laser Scanning Photostimulation and Fast Dye Imaging, Laser Scanning, Theory and Applications, Prof. Chau-Chang Wang (Ed.), ISBN: 978-953-307-205-0, InTech, Available from: http://www.intechopen.com/books/laser-scanning-theory-and-applications/high-precision-and-fast-functional-mapping-of-brain-circuitry-through-laser-scanning-photostimulatio

INTECH
open science | open minds